Human Identification from at-a-distance Face Images using Sparse Representation of Local Iris Features

Ajay Kumar, Tak-Shing Chan, Chun-Wei Tan
Department of Computing, The Hong Kong Polytechnic University, Kowloon, Hong Kong
Email: ajaykr@ieee.org, cstchan@comp.polyu.edu.hk, cscwtan@comp.polyu.edu.hk

Abstract

Automated human identification at-a-distance, using completely automated iris segmentation, is highly challenging and has wide range of civilian and forensics applications. Iris images acquired at-a-distance using visible and infrared imaging are often noisy and suffer from divergent spectral changes largely resulting from scattering, albedo and spectral absorbance selectivity. Therefore further research efforts are required to develop feature extraction techniques which are more tolerant to illumination changes and noise. This paper develops a new approach for the automated recognition from such distantly acquired iris images using sparse representation of local Radon transform (LRT) based orientation features. We model the iris representation problem as sparse coding solution based on computationally efficient LRT dictionary which is solved by widely studied convex optimization approach/strategy. The iris recognition and verification performance for the distantly acquired iris images are also evaluated using baseline 1-D log-Gabor filter and monogenic log-Gabor filter based approach. The experimental results are reported on the publically available UBIRIS V2, FRGC and CASIAV4-distance databases. The achieved experimental results on at-a-distance databases are highly promising and confirm the usefulness of the approach.

1. Introduction

Human identification using automated iris recognition has emerged as one of the most popular technologies for its wide applications in national ID cards and immigration control at border crossings. Iris texture in humans is known to be highly unique, even in case of identical twins and even between left and right eyes of an individual. Currently deployed iris recognition technologies achieve remarkable accuracies but operate on high quality images acquired under near infrared illumination from close distances [4]. Some recently developed solutions are now commercially available to identify subject's at-a-distance. Sri International has introduced iris-on-the-move (IOM) system which can recognize iris from the stand-off distance of three meters while subjects walk though near infrared illumination panels. Excessive levels of near infrared illumination can be hazardous for human eyes. Such concerns are largely attributed to the fact that the human eyes fail to respond and protect itself from the near infrared illumination using the autonomic responses like blinking and aversion often generated for the excessive visible illumination. Therefore further advances are needed to develop iris recognition technologies which can operate in less constrained environment at increased standoff distances and under visible illumination.

Table 1. Iris Recognition from increased *stand-off distances* in variable illumination bands.

	 **Visible Illumination**	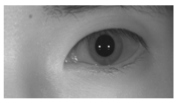 **Near Infrared Illumination**
Remote Surveillance	High	Low
Recognition Accuracy	Low	High
Applications	Forensics, Surveillance	Access Control, High Security
Imaging Cost	Low	High
Image quality	Degraded (High Noise)	Good
Medical/health concern	Low	High
User Cooperation	Low	High
Key Challenges	**Imaging Quality/Resolution, Robust Iris Segmentation and Feature Extraction**	Safe Imaging/Illumination, Segmentation/Recognition are Relatively Matured

Recent research efforts to achieve iris recognition from visible wavelength illumination and from distantly acquired images have delivered exciting results. The research group at the University of Beira Interior, Portugal, have released two versions of iris image databases which have been acquired using visible illumination imaging at-a-distance (4 to 8 meters), and organized NICE I [7] and NICE II [8] competitions to promote research efforts in this direction. There are now several quality publications that detail various algorithms that were developed to segment [4], [14] and more recently recognize [15], [17]-[18], [25], iris images from acquired from such less-constrained environment. Automated segmentation of such (noisy) iris images is highly challenging as these images are often accompanied by noise resulting from (multiple) source reflection, defocus, eye glasses, and occlusions resulting from pose, eyelash, hair and off-angle images. The recognition of such visible illumination segmented iris images is also highly challenging largely due to varying iris pixel resolution, varying/low image contrast resulting from varying iris pigmentation, illumination, scattering, albedo, absorption selectivity and shadows. Therefore further efforts are required to develop robust feature extraction and matching strategies for visible illumination iris images that

can accommodate and account for such image variations from increased standoff distances in real environment.

1.1. Our Work

This paper investigates a new approach for robust iris recognition from visible illumination face images acquired in less constrained imaging environment. The developed approach attempts to extract orientation specific information from the randomly distributed iris texture features which are commonly observed in the visible illumination iris images. Our feature extraction scheme exploits the sparse representation of the finite Radon transform based local orientation information. The idea is inspired from the success of orientation information in [21], [22] and also for the iris recognition in [2], computational simplicity of localized Radon transform, and growing success in sparse representation of biometric features [9], [16], [23]. The similarity between the query and gallery templates is computed from the minimum matching distance that can account for the commonly observed variations resulting from translation and rotation of eyes in distantly acquired images. The iris recognition and verification performance from such distantly acquired iris images are also evaluated using baseline 1-D log-Gabor filter [13] based approach. We also experimented with monogenic quadrature filters [24] to ascertain their advantage over 1-D log-Gabor filter based feature extraction. The experimental results are reported on the publically available, UBIRIS V2 [3], CASIA V4 [6] and FRGC [12] databases. The experimental results, both for the verification and recognition, achieve significantly improved performance over those from the baseline approaches and suggest the expectations from distantly acquired iris images for surveillance and forensics applications. We also present experimental results to ascertain the robustness of this approach on two conventional near infrared iris databases, *i.e.*, CASIA V3 and IITD V1, acquired at close distances.

2. Sparse Representation of Local Texture Orientation Features

The local texture information from the distantly acquired images is often visible in furrows, crypts, freckles and arching ligaments. The appearance and contrast of such localized texture details is known to vary with the level of iris pigmentation [3]-[4]. One possible approach to represent the local distribution of such random texture constituents is to compute their spatial orientation across multiple scales. Such spatial orientation information is popularly acquired using the convolution with the multiscale and multiorientation filters. However the convolution with such filters, *e.g.* Gabor filters or second Derivative of Gaussian, is computationally expensive and therefore we construct an overcomplete dictionary using a set of binarized masks which are designed to recover the localized orientation information from the unwrapped iris images. The elements of this dictionary $\boldsymbol{D}$ are defined by $[\boldsymbol{d}_1, \dots, \boldsymbol{d}_K] \in \mathbf{R}^{n \times K}$ with $k \leq n$. In this work, the elements of dictionary $\boldsymbol{D}$, *i.e.*, $\boldsymbol{d}$, are designed to estimate spatial orientation of local textured details in one of the possible directions as shown in figure 1. These elements are constructed from a set of points L_θ on a finite grid R_q^2, where $R_q = \{0, 1, \dots, q-1\}$ with q as a positive integer, and defined as follows:

$$L_\theta = \begin{cases} \{(x,y) | y = \tan(\theta) \times (x - x_0) + y_0, x \in R_q\}, & \theta \neq \frac{\pi}{2} \\ \{(x,y) | x = x_0, y \in R_q\}, & \theta = \frac{\pi}{2} \end{cases} \quad (1)$$

where $\theta \in [0, \pi)$ and denotes the angle between line L_θ and the positive x-axis, and L_θ is the line passing through the centre (x_0, y_0) of R_q^2 [2].

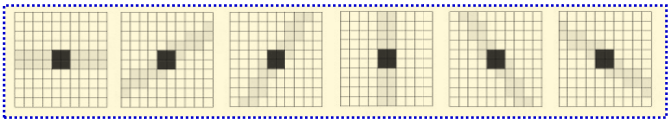

Figure 1: Computing the localized orientation of iris texture shapes using binarized LRT masks in a 10 × 10 pixel region in the directions of 0°, π/6, π/3, π/2, 2π/3, 5π/6 and the L_θ is 2 pixel wide.

This approach is inspired by recent advances and exciting results in the sparse representation of biometrics features [9], [16], [23]. We use sparse representation to model computationally efficient LRT based dictionary which encodes spatial orientation of localized iris constituent features. The sparse representation uses image patches uniformly sampled from the unwrapped iris image, with adjacent patch centers of $l \times l$ LRT mask. For each vectorized patch $\boldsymbol{g}_{x,y} \in \mathbf{R}^n$ centered at (x, y), the sparse representation, *i.e.* coefficients $\boldsymbol{\alpha}_{x,y}$, requires solution for the following l_1-regularized optimization problem:

$$\min_{\boldsymbol{\alpha}_{x,y}} \left\| \boldsymbol{D}\boldsymbol{\alpha}_{x,y} - \boldsymbol{g}_{x,y} \right\|_2^2 + \lambda \left\| \boldsymbol{\alpha}_{x,y} \right\|_1 \quad (2)$$

The solution to above problem can be generated by well studied convex optimization approaches detailed in the literature. In this work we use fast iterative shrinkage thresholding algorithm (FISTA) [26] as it is significantly faster. The magnitude of λ is empirically selected and fixed as $\lambda = 0.02$ for all the experiments in this paper. All the negative $\boldsymbol{\alpha}_{x,y}$'s are then clipped to zeros and the resulting (clipped) coefficients from the same orientation of LRT dictionary are added to compute representative orientation of the feature $\boldsymbol{\varphi}_{x,y}(\theta)$. The index of the dominant orientation is binary encoded to extract the feature template. This process is repeated for every patch in the unwrapped iris image to extract sparse representation of LRT based localized orientation details. This algorithm (for bright or white pixels) can be summarized as in the following;

Algorithm 1 Sparse Representation of Local Orientation Features

Input: $\boldsymbol{D}, \boldsymbol{g}_{x,y} \forall x, y$

Output: $\mathbf{T}_{xy} \forall x, y$

1: **for** each patch $\boldsymbol{g}_{ij}$

2: Sparse Representation from LRT Dictionary

$$\boldsymbol{\alpha}^{*}_{xy} = \min_{\alpha_{xy}} \left\| \boldsymbol{D}\boldsymbol{\alpha}_{xy} - \boldsymbol{g}_{xy} \right\|_2^2 + \boldsymbol{\lambda} \left\| \boldsymbol{\alpha}_{xy} \right\|_1$$

3: Clipping and Summation

$$\boldsymbol{\varphi}_{xy}(\boldsymbol{\theta}) = \sum_{\boldsymbol{same\ orientation}} \max\left(\mathbf{0}, \boldsymbol{\alpha}^{*}_{xy}\right) \forall \boldsymbol{\theta}$$

4: Feature Template using Dominant Orientation Estimation

$$\mathbf{T}(x, y) = \arg\max_{\theta} \boldsymbol{\varphi}_{xy}(\boldsymbol{\theta})$$

5: **end**

2.1. Generating Matching Scores

The matching scores between the two iris feature templates R and T, with their corresponding masks M_R and M_T, is generated similar manner as in the following [2]:

$$Score(R, T, M_R, M_T) = \min_{\forall i \in [0,2w], \forall\, j \in [0,2h]} \left(\frac{\sum_{x=1}^{m} \sum_{y=1}^{n} \psi\left(\hat{\boldsymbol{R}}(x+i, y+j), \boldsymbol{T}(x,y), M_R(x+i, y+j), M_T(x,y)\right)}{\sum_{x=1}^{m} \sum_{y=1}^{n} M_R(x,y) \cap M_T(x,y)} \right) \quad (3)$$

where $\hat{R}$ is the registered feature template with the width and height expanded to $2w + m$ and $2h + n$, while

$$w = floor\left(\frac{m}{t_w}\right),\ h = floor\left(\frac{n}{t_h}\right) \quad (4)$$

$$\hat{\boldsymbol{R}}(x, y) = \begin{cases} R(x-w, y-h) & x \in [w+1, w+m],\ y \in [h+1, h+n] \\ -1 & otherwise \end{cases} \quad (5)$$

$$\psi(J, K, M, N) = \begin{cases} 0 \ if\ M = N = 1\ and\ J = K \neq -1\ or\ J = -1 \\ 1 \quad otherwise \end{cases} \quad (6)$$

We divide the template images, *i.e.* $T(x, y)$, into disjoint sub-regions which are matched using equation (6). Thus our matching strategy [19] attempts to account the influence of local image variations by matching the corresponding template sub-regions with a small amount of shifting. Therefore this approach is expected to be more robust against the image variations which are more common in the noisy iris images acquired using at-a-distance imaging.

3. Experiments

The experimental results from the proposed approach for matching distantly acquired iris images are presented on three publicly available databases; (i) UBIRIS V2 [3], (ii) FRGC [6] and CASIA V4 [12]. The first two databases are acquired using visible illumination imaging while the CASIA V4 database is acquired at-a-distance but using near infrared illumination. The performance of this approach is also evaluated on publicly available CASIA V3 and IITD v1 databases.

The imaging distance for UBIRIS V2 database ranges from 4-8 meters and we employed 1000 images from 171 subjects for the experiments. This dataset is same as released for the NICE II competition [8]. The experimental results are illustrated on the independent test data consisting of 904 images from 152 subjects as illustrated in table 2.

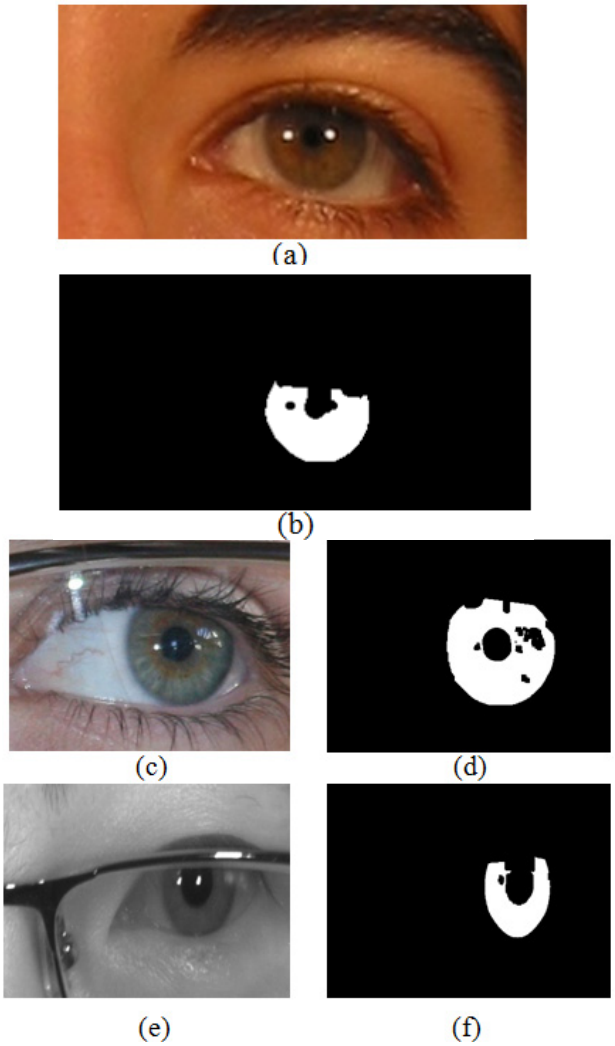

Figure 2: Image samples from at-a-distance iris databases along with their respective automatically generated iris segmentation masks; FRGC in (a)-(b), UBIRISV2 in (c)-(d), and CASIA V4 at-distance in (e)-(f).

The FRGC dataset, which comprises of high resolution still images, is also investigated to ascertain matching performance. The images used in our experiments are selected from the session 2002-269 to 2002-317 of 'Fall2002'. We employed completely automated approach for extracting *left* eye images from FRGC face images using the same approach as detailed in [10] or [14]. The iris diameters from the extracted eyes using this dataset do not meet minimum requirement of 200 pixels suggested by ISO Standard ISO/IEC 19794-6 [11], or even 140 pixels suggested in [5]. Therefore we automatically removed those automatically detected eye-pair regions which do not meet minimum size of 300 × 150 pixels (determined empirically). The selection of independent test images from 150 subjects and the details on the employed training set are illustrated in table 2.

We also employed CASIA V4 dataset which consists of 2567 iris images acquired from three meters of standoff distance. Similar to FRGC dataset, the detection of faces and eyes from this publicly available dataset was also performed automatically and the resulting images were employed for recognition experiments using the independent test data from 131 subjects as summarized in table 2.

We employed the approach detailed in [18] for the automated segmentation of the iris images from the eye images in the three dataset. Figure 2 illustrates the sample iris/eye images from these three dataset and their respective segmented results. The size of unwrapped iris images was 512 × 64 pixels for UBIRIS V2 and CASIA V4 database while it was 256 × 32 pixels for FRGC database. We employed leave-one-out strategy to ascertain average of experimental results from the independent test data. This approach generated 904 genuine and 136504 impostor matching scores for UBIRIS V2, 500 genuine and 74500 impostor matching scores for FRGC, and 900 genuine and 122047 impostor scores from the experiments. The parameters for the algorithm, *i.e.* the line width *w* and mask size *l*, were automatically extracted from the independent training data (table 2) and is detailed in Appendix A.

Table 2. Distribution of train/test images for three databases in our experiments.

Database	UBIRIS.v2	FRGC	CASIA.V4
No. of test images	904	500	961
No. of test subjects	152	150	131
No. of train images	96	40	79
No. of train subjects	19	13	10

4. Results

The experimental results for the recognition experiments are firstly presented using respective the cumulative match characteristics (CMC). The receiver operating characteristics (ROC) is employed is employed to evaluate the verification performance and is also presented in the following sections.

4.1 Results from the Recognition Experiments

The average cumulative match characteristics from the recognition experiments using UBIRIS V2 database is shown in figure 3 (a). This figure also illustrates the corresponding performance when monogenic log Gabor and 1-D log Gabor are employed for the verification experiments. The template size for the 1-D log Gabor filters is two bits per pixel while the monogenic (quadtature) log Gabor filters log Gabor filters generate template size of three bits per pixel. The matching distance between the binarized iris image template for the monogenic log Gabor is also be computed using the normalized Hamming distance (like those for 1-D log Gabor filter based approach).

The experimental results in figure 3 suggest that the sparse representation of local orientation features can achieve significant improvement in rank-one recognition

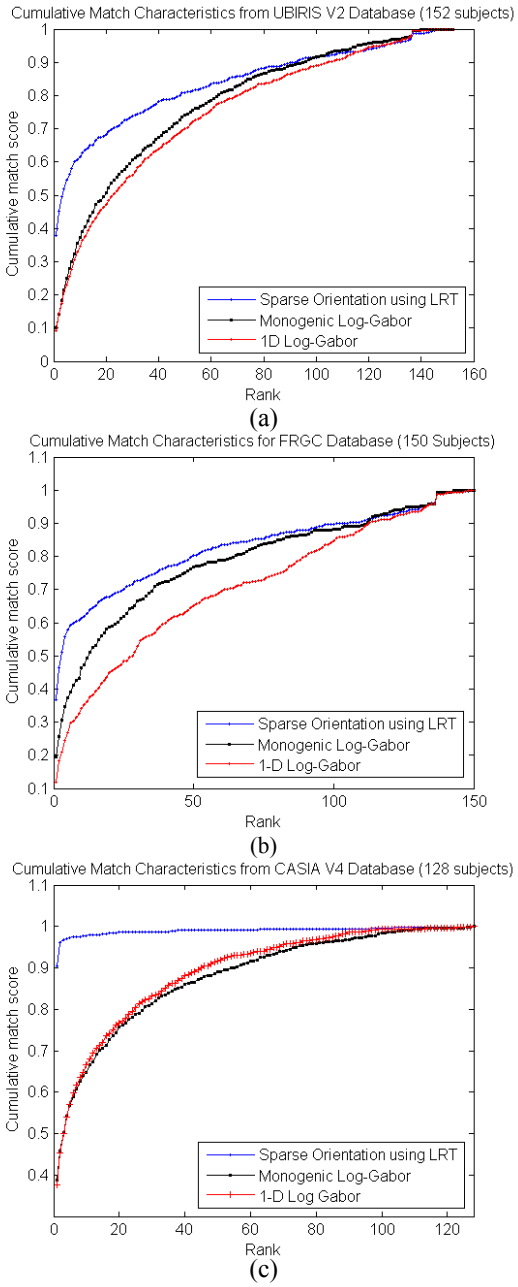

Figure 3: Cumulative Match Characteristics using from distantly acquired iris images using (a) UBIRIS V2, (b) FRGC, and (c) CASIA V4 at-distance database.

accuracy for all the three different dataset considered in the experiments. The rank-one recognition accuracy achieved from CASIA V4 (90.43%) is the highest while those from the FRGC dataset (33.2%) is the lowest.

4.2 Results from the Verification Experiments

The receiver operating characteristics from the authentication experiments using UBIRIS V2 database is

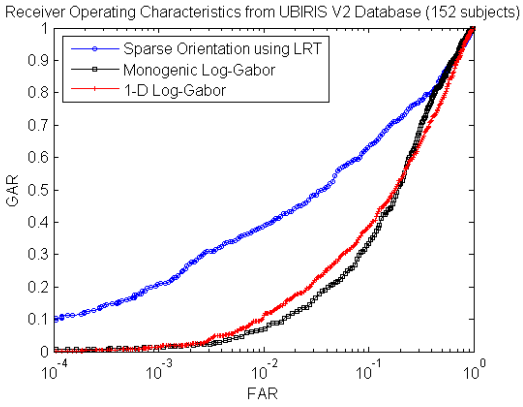

(a)

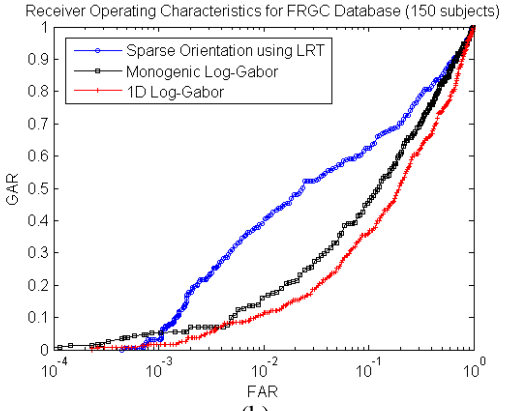

(b)

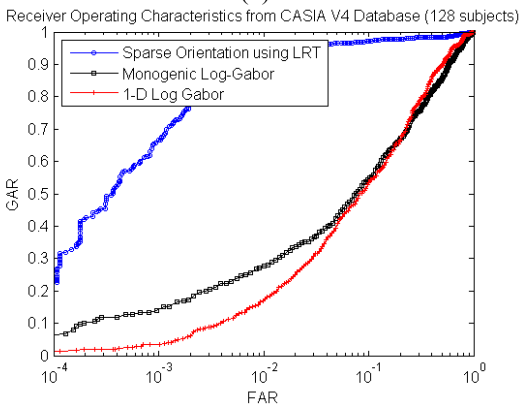

(c)

Figure 4: Receiver Operating Characteristics using from distantly acquired iris images using (a) UBIRIS V2, (b) FRGC, and (c) CASIA V4 at-distance database.

is shown in figure 4(a). This figure also illustrates the corresponding performance when monogenic log Gabor and 1-D log Gabor are employed for the verification experiments. The experimental results in figure 4 suggest that the sparse representation of local orientation features generate significant improvement in the performance for the verification experiments similar to those trends observed from the recognition experiments.

4.3 Results from the Other Iris Databases

In order to ascertain the performance from the sparse representation of local orientation features, we performed experiments on *low resolution iris images* which are available in IITDv1 database [27]. Figure 5 illustrates the CMC plots and the ROC plots from the experiments on all the 224 subject dataset (1120 images) using leave-one-out strategy and generating average of results. The image segmentation, unwrapping and enhancement steps were same as detailed in [20] and resulted in 48 × 432 pixels images for the feature extraction. The experimental results, both from the verification and recognition experiments, are quite promising (achieve rank-one accuracy of 99.01% and equal error rate of 0.71%).

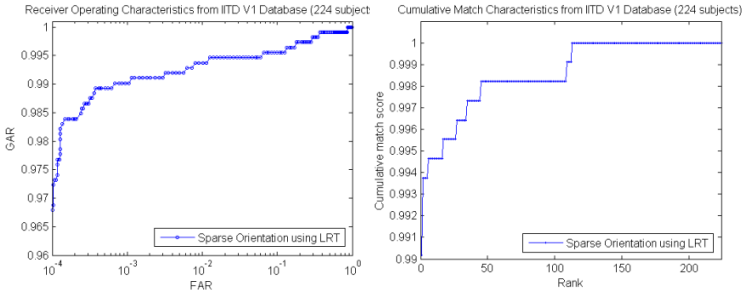

Figure 5: Receiver Operating Characteristics and Cumulative Match Characteristics using IITDv1 iris database.

We also evaluated performance of the developed approach using CASIA V3 database (left eyes) from all the 411 subjects in the database. We employed first seven images from each of the 411 subjects (2877 images) for the experiments. The image segmentation, unwrapping and enhancement steps were similar as detailed in [20] and resulted in 64 × 512 pixel images for the feature extraction. The number of genuine scores from this experiments were 2466 (411 × 6) and the number of imposter matches were 1,011,060 (411 × 410 × 6). The experimental results achieve average rank-one recognition accuracy of 93.81% and equal error rate of 3.96%. The results in figure 5-6 suggest effectiveness of this approach even for the near infrared iris databases acquired from the close distances.

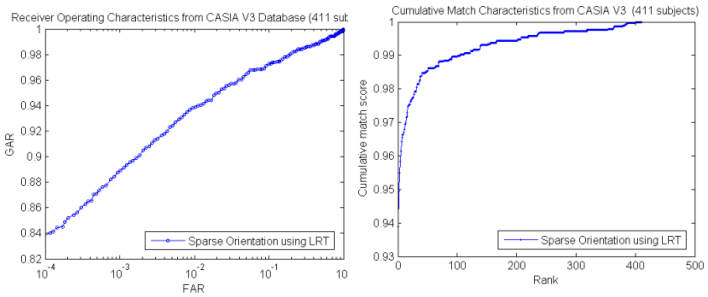

Figure 6: Receiver Operating Characteristics and Cumulative Match Characteristics using CASIA V3 iris database.

5. Conclusions and Further Work

This paper has investigated a new approach for at-a-distance iris recognition using sparse representation of local texture features. The experimental results are presented on three publicly available databases, *i.e*., UBIRIS V2, FRGC, and CASIA V4, both for the recognition and verification experiments. These experimental results illustrate significant improvement over two baseline approaches (using 1-D log Gabor and monogenic log Gabor filter) considered in this work. One of the key advantages of selecting the Radon transform based dictionary for sparse representation is related to it's the computational simplicity as it just requires simple summation operations. Another favorable factor for using this dictionary lies in the significantly reduced template size as the LRT operations have associated down sampling effect which reduces the template size by a factor of w^2 (w is line width) as compared to those using Gabor, sDoG or other spatial filters.

The experimental results from the visible illumination at-a-distance imaging databases, *i.e*. UBIRIS V2 and FRGC, databases are quite promising but not yet matured for real applications. The average rank-one recognition accuracy from these two, at-a-distance visible illumination imaging, databases is poor and may only be suitable for surveillance and forensic applications. The reason for this can primarily be attributed to the imaging resolution. According to the ISO Standard 19794-6 for iris data [11], the iris diameter should be at least 200 pixels. However, the average iris diameter from both of these two databases fails to meet such criteria. Our experiments have estimated that the average iris diameter from FRGC is ~ 62 pixels (61.72, much less than half of the requirement suggested in [5]) while those from UBIRIS V2 database is ~123 (122.48) pixels. The average iris diameter from these two databases was generated using the ground truth masks employed in earlier study [14]. In our experiments, we did not make any attempt to discriminate or reject iris images based on imaging resolution or quality, primarily to benchmark and ensure repeatability of the experiments. Recent publications [17]-[18] have also explore at-a-distance iris verification but only on the UBIRIS database. The experimental results presented in this paper from the verification experiments on UBIRIS database compare quite favorably, *e.g*. with [15] using co-occurrence phase histograms or with [17] using LBP, in terms of complexity, template size or performance. However one to one such comparison may be quite difficult due to lack of details on the training parameters in some of such recent publications.

The addition of periocular features in the face image matching has shown [10] to significantly improve the face recognition performance. However, in the best of our knowledge, the possibility of iris recognition from this distantly acquired face image dataset has not yet been attempted. Such experiments have been presented in this paper and suggest that iris recognition from FRGC dataset is also feasible and can possibly be used to further improve the performance for the face recognition. Our experiments in this paper have only employed single-scale sparse representation of orientation features, primarily to limit the computations. However the multi-scale sparse representation of LRT based orientation features, as explored in [2], is expected to further improve the performance and is suggested for further work.

6. Acknowledgement

This work is partially supported by the research grant from the Department of Computing, The Hong Kong Polytechnic University, grant no. A-PJ70.

7. References

[1] T. Tan, Z. He, and Z. Sun, "Efficient and robust segmentation of noisy iris images for non-cooperative iris recognition," *Image & Vision Comput.*, vol. 28, no. 2, pp. 223–230, Feb. 2010.

[2] Y. Zhou and A. Kumar, "Personal identification from iris images using localized Radon transform," *Proc. ICPR 2010,* Istanbul, Aug. 2010.

[3] H. Proença S. Filipe, R. Santos, J. Oliveira, and L. Alexandre, "The UBIRIS.v2: A database of visible wavelength images captured on the move and at-a-distance," *IEEE Trans. Pattern Anal. Mach. Intell.*, vol. 32, pp. 1529–1535, 2010.

[4] H. Proenca, "Iris recognition: On the segmentation of degraded images acquired in the visible Wavelength," *IEEE Trans. Pattern Anal. Mach. Intell.*, vol. 32, no. 8, pp. 1502–1516, 2010.

[5] J. Daugman, "How iris recognition works," *IEEE Trans. Circuits Syst. Video Technol.*, vol. 14, no. 1, pp. 21–30, 2004.

[6] CASIA Iris Database version 3.0. http://www.cbsr.ia.ac.cn/english/IrisDatabase.asp

[7] NICE.I - Noisy Iris Challenge Evaluation, Part I. http://nice1.di.ubi.pt/index.html

[8] NICE:II - Noisy Iris Challenge Evaluation, Part II. http://nice2.di.ubi.pt/

[9] D. Xu, Y. Huang, Z. Zeng, and X. Xu, "Human gait recognition using patch distribution feature and locality-constrained group sparse representation," *IEEE Trans. Image Processing*, vol. 21, pp.316-326, Jan. 2012.

[10] U. Park, R. R. Jillela, A. Ross, and A. K. Jain, "Periocular biometrics in the visible spectrum," *IEEE Trans. Info. Forensics & Security*, vol. 6, pp. 96–106, 2011.

[11] ISO/IEC 19794-6:2005. Information technology -- Biometric data interchange formats -- Part 6: Iris image data.

[12] Face Recognition Grand Challenge – Overview. http://www.frvt.org/FRGC/

[13] L. Masek, *MATLAB source code for a biometric identification system based on iris patterns*, 2003 http://www.csse.uwa.edu.au/~pk/studentprojects/libor/index.html

[14] C.-W. Tan and A. Kumar, "Automated segmentation of iris images using visible wavelength face images," *Proc. CVPR 2011*, pp. 9-14, Colorado Springs, CVPRW'11, June 2011.

[15] P. Li, Z. Liu and N. Zhao, "Weighted co-occurrence phase histogram for iris recognition," *Pattern Recognition Letters*, 2011, doi:10.1016/j.patrec.2011.06.018

[16] J. Wright, A. Yang, A. Ganesh, S. Sastry, and Y. Ma, "Robust face recognition via sparse representation," *IEEE Trans. Pattern Anal. Mach. Intell.*, pp. 210-227, Feb. 2009.
[17] M. De Marsico, M. Nappi and D. Riccio, "Noisy iris recognition integration scheme," *Pattern Recognition Letters*, 2011, doi: 10.1016/j.patrec.2011.09.010
[18] T. Tan, X. Zhang, Z Sun, and H. Zhang, "Noisy iris image matching by using multiple cues," *Pattern Recognition Letters*, 2011, doi: 10.1016/j.patrec.2011.08.009
[19] Y. Zhou and A. Kumar, "Human identification using palm vein images," *IEEE Trans. Information Forensics & Security,* vol. 6, no. 4, pp. 1159-1274, Dec. 2011.
[20] A. Kumar and A. Passi, "Comparison and combination of iris matchers for reliable personal authentication," *Pattern Recognition*, vol. 43, no. 3, pp. 1016–1026, 2010.
[21] A. Kumar and Y. Zhou, "Human identification using KnuckleCodes," *Proc. BTAS 2009*, pp. 147-152, Sep. 2009.
[22] W. Jia, D.-S. Huang, and D. Zhang, "Palmprint verification based on robust line orientation code," *Pattern Recognition,* vol. 41, no. 5, pp. 1504-1513, May, 2008.
[23] W. Zuo, Z. Lin, Z. Guo, and D. Zhang, "The multiscale competitive code via sparse representation for palmprint verification," *Proc. CVPR 2010,* pp. 2265-2272, Jun. 2010.
[24] P. Kovesi, Matlab and Octave Functions for Computer Vision and Image Processing, Matching image phase points using monogenic phase data, http://www.csse.uwa.edu.au/~pk/research/matlabfns/Match/matchbymonogenicphase.m 2005
[25] K. Y. Shin, G. P. Nam, D. S. Jeong, D. H. Cho, D. H. Kang, K. R. Park, and J. Kim, "New iris recognition method for noisy iris images," *Pattern Recognition Letters*, 2011, doi: 10.1016/j.patrec.2011.08.016
[26] A. Beck and M. Teboulle, "A fast iterative shrinkage thresholding algorithm for linear inverse problem," *SIAM Journal on Imaging Sciences*, vol. 2, pp. 183–202, 2009.
[27] IIT Delhi Iris Database version 1.0, http://web.iitd.ac.in/~biometrics/DatabaseIris.htm

Appendix A

The parameters for the evaluation of independent test dataset were selected from the training database as detailed in table 2. The selection of parameters for each of the three databases is illustrated in the following where R1RR denotes the average rank-one recognition accuracy, EER denotes average equal error rate from the corresponding (training) dataset.

UBIRIS V2

Sparse Orientation using LRT

w	1		2	3	
l	19	21	20	19	21
R1RR (%)	57.2917	57.2917	63.5417	52.0833	58.3333

Best parameters: w = 2, l = 20, R1RR = 63.5417%.

Monogenic Log-Gabor

β \ λ		42	44	46	48
0.5	R1RR (%)	35.4167	41.6667	41.6667	39.5833
	EER (%)	29.4444	28.3918	28.4211	29.4152
1.0	R1RR (%)	42.7083	43.7500	43.7500	42.7083
	EER (%)	27.7193	27.3977	28.1287	27.3977
1.5	R1RR (%)	39.5833	40.6250	38.5417	38.5417
	EER (%)	30.7310	30.5263	27.6023	27.3684

Best parameters: λ = 44, β = 1.0 octaves, R1RR = 43.7500%, EER = 27.3977%.

1-D Log-Gabor

β \ λ	24	26	28
2.5	27.0833	29.1667	30.2083
3.0	35.4167	36.4583	34.3750
3.5	29.1667	26.0417	25.0000

Best parameters: λ = 26, β = 3.0 octaves, R1RR = 36.4583%.

FRGC

Sparse Orientation using LRT

w	2		3	4	
l	16	18	17	16	18
R1RR (%)	57.5000	45.0000	60.0000	52.5000	50.0000

Best parameters: w = 3, l = 17 (no change), R1RR = 60.0000%.

Monogenic Log-Gabor

β \ λ		27	28	29	30
2.5	R1RR (%)	55.0000	57.5000	57.5000	60.0000
	EER (%)	26.8750	22.7083	22.7083	24.5833
3.0	R1RR (%)	60.0000	62.5000	62.5000	60.0000
	ERR (%)	22.3958	22.3958	22.5000	22.5000
3.5	R1RR (%)	52.5000	52.5000	55.0000	55.0000
	EER (%)	27.6042	27.6042	27.5000	27.5000

Best parameters: λ = 28, β = 3.0 octaves, R1RR = 62.5000%, EER = 22.3958%.

1-D Log-Gabor

β \ λ		22	23	24	25
1.0	R1RR (%)	45.0000	50.0000	52.5000	47.5000
	EER (%)	30.0000	28.1250	27.5000	30.0000
1.5	R1RR (%)	57.5000	60.0000	60.0000	55.0000
	EER (%)	30.0000	28.6458	27.5000	27.5000
2.0	R1RR (%)	52.5000	52.5000	52.5000	50.0000
	EER (%)	25.0000	25.0000	27.6042	27.5000

Best parameters: λ = 24, β = 1.5 octaves, R1RR = 60.0000%, EER = 27.5000%

CASIA V4

Sparse Orientation using LRT

w	1	2		3
l	31	30	32	31
R1RR (%)	96.2025	96.2025	92.4051	91.1392
EER (%)	7.5949	8.8608	6.3291	5.2039

Best parameters: w = 1, l = 31, R1RR = 96.2025%, EER = 7.5949%.

Monogenic Log-Gabor

β \ λ	24	26	28
1.5	73.4177	74.6835	75.9494
2.0	75.9494	79.7468	77.2152
2.5	72.1519	74.6835	69.6203

Best parameters: λ = 26, β = 2.0 octaves, R1RR = 79.7468%.

1-D Log Gabor

β \ λ	36	38	40
3.0	75.9494	73.4177	74.6835
3.5	77.2152	79.7468	77.2152
4.0	72.1519	72.1519	72.1519

Best parameters: λ = 38, β = 3.5 octaves, R1RR = 79.7468%.